Towards a synchronization theory of microwave-induced zero-resistance states

O. V. Zhirov,[1] A. D. Chepelianskii,[2] and D. L. Shepelyansky[3]
[1]*Budker Institute of Nuclear Physics, 630090 Novosibirsk, Russia*
[2]*Cavendish Laboratory, Department of Physics, University of Cambridge, CB3 0HE, United Kingdom*
[3]*Laboratoire de Physique Théorique du CNRS, IRSAMC, Université de Toulouse, UPS, 31062 Toulouse, France*
(Received 12 February 2013; revised manuscript received 27 April 2013; published 3 July 2013)

We develop a synchronization theory for the dynamics of two-dimensional electrons under a perpendicular magnetic field and microwave irradiation showing that dissipative effects can lead to the synchronization of the cyclotron phase with the driving microwave phase at certain resonant ratios between microwave and cyclotron frequencies. We demonstrate two important consequences of this effect: the stabilization of skipping orbits along the sample edges and the trapping of the electrons on localized short-ranged impurities. We then discuss how these effects influence the transport properties of ultrahigh-mobility two-dimensional electron gas and propose mechanisms by which they lead to microwave-induced zero-resistance states. Our theoretical analysis shows that the classical electron dynamics along the edge and around circular disk impurities is well described by the Chirikov standard map providing a unified formalism for those two rather different cases. We argue that this work will provide the foundations for a full quantum synchronization theory of zero-resistance states for which a fully microscopic detailed theory still should be developed.

DOI: 10.1103/PhysRevB.88.035410 PACS number(s): 73.40.−c, 05.45.−a, 72.20.My

I. INTRODUCTION

The experiments on resistivity of high-mobility two-dimensional electron gas (2DEG) in the presence of a relatively weak magnetic field and microwave radiation led to a discovery of striking zero-resistance states (ZRS) induced by a microwave field by Mani *et al.*[1] and Zudov *et al.*[2] Other experimental groups also found the microwave-induced ZRS in various 2DEG samples (see, e.g., Refs. 3–5). A similar behavior of resistivity is also observed for electrons on a surface of liquid helium in the presence of magnetic and microwave fields.[6,7] These experimental results obtained with different systems stress the generic nature of ZRS. Various theoretical explications for this striking phenomenon have been proposed during the decade after the first experiments.[1,2] An overview of experimental and theoretical results is give in a recent review.[8]

In our opinion the most intriguing feature of ZRS is their almost periodic structure as a function of the ratio $j = \omega/\omega_c$ between the microwave frequency ω and cyclotron frequency $\omega_c = eB/mc$ (in the following we are using units with electron charge e and mass m equal to unity). Indeed, the Hamiltonian of electrons in a magnetic field is equivalent to an oscillator; it has a magnetoplasmon resonance at $j = 1$ but in a linear oscillator there are no matrix elements at $j = 2,3,\ldots$ and hence a relatively weak microwave field is not expected to affect electron dynamics and resistivity properties of transport. Of course, one can argue that impurities can generate harmonics being resonant at high $j > 1$ but ZRS is observed only in high-mobility samples and thus the density of impurities is expected to be rather low. It is also important to note that ZRS appears at high Landau levels $\nu \sim 50$ so that a semiclassical analysis of the phenomenon seems to be rather relevant.

In this work we develop the theoretical approach proposed in Ref. 9. This approach argues that impurities produce only smooth potential variations inside a bulk of a sample so that ZRS at high j appear from the orbits moving along sharp sample boundaries. It is shown[9] that collisions with boundaries naturally generate high harmonics and that a moderate microwave field gives stabilization of edge channel transport of electrons in a vicinity of $j \approx j_r = 1 + 1/4, 2 + 1/4, 3 + 1/4, \ldots$ producing at these j a resistance going to zero with increasing microwave power. This theory is based on classical dynamics of electrons along a sharp edge. The treatment of relaxation processes is modeled in a phenomenological way by a dissipative term in the Newton equations. An additional noise term in the dynamical equations takes into account thermal fluctuations. The dissipation leads to synchronization of the cyclotron phase with a phase of microwave field producing stabilization of edge transport along the edges in the vicinity of resonant j_r values. Thus, according to the edge stabilization theory[9] the ZRS phase is related to a universal synchronization phenomenon which is a well-established concept in nonlinear sciences.[10]

While the description of edge transport stabilization[9] captures a number of important features observed in ZRS experiments it assumes that the contribution of bulk orbits in transport is negligibly small. This assumption is justified for smooth potential variations inside the bulk of a sample. However, the presence of isolated small-scale scatterers inside the bulk combined with a smooth potential component can significantly affect the transport properties of electrons (see, e.g., Ref. 11). Also the majority of theoretical explanations of the ZRS phenomenon considers only a contribution of scattering in a bulk.[8] Thus it is necessary to analyze how a scattering on a single impurity is affected by a combined action of magnetic and microwave fields. In this work we perform such an analysis modeling impurity by a rigid circular disk of finite radius. We show that the dynamics in the vicinity of a disk has significant similarities with the dynamics of orbits along a sharp edge leading to the appearance of ZRS-type features in a resistivity dependence on j.

The paper is composed as follows: In Sec. II we discuss the dynamics in the edge vicinity; in Sec. III we analyze scattering on a single disk; in Sec. IV we study scattering on many disks

 ©2013 American Physical Society

when their density is low—here we determine the resistivity dependence on j and other system parameters. Physical scales of ZRS effects are analyzed in Sec. V; the effects of two microwave driving fields and other theory predictions are considered in Sec. VI; and discussion of the results is given in Sec. VII.

We study various models which we list here for the reader's convenience: the wall model described by the Newton equations (1) and (2) with microwave field polarization perpendicular to the wall [model (W1) equivalent to model (1) in Ref. 9]; the Chirikov standard map description (3) of the wall model dynamics called model (W2) [equivalent to model (2) in Ref. 9 at parameter $\rho = 1$]; the single-disk model with radial microwave field called model (DR1); the Chirikov standard map description (3) of model (DR1) called model (DR2) [here $v_y \to v_r$ in (3), $\rho > 1$]; the model of a single disk in a linearly polarized microwave field and static electric field called model (D1); the model of transport in a system with many disks called model (D2) which extends model (D1); an extension of model (D2) with disk roughness and dissipation in space called model (D3); the wall model (W2) extended to two microwave fields is called model (W3).

II. DYNAMICS IN EDGE VICINITY

We recall first the approach developed in Ref. 9. Here, the classical electron dynamics is considered in the proximity of the Fermi surface and in the vicinity of the sample edge modeled as a specular wall. The motion is described by Newton equations

$$d\mathbf{v}/dt = \omega_{\mathbf{c}} \times \mathbf{v} + \omega\vec{\epsilon}\cos\omega t - \gamma(v)\mathbf{v} + I_{ec} + I_s, \quad (1)$$

where a dimensionless vector $\vec{\epsilon} = e\mathbf{E}/(m\omega v_F)$ describes microwave driving field $\mathbf{E}$. Here an electron velocity v is measured in units of Fermi velocity v_F and $\gamma(v) = \gamma_0(|\mathbf{v}|^2 - 1)$ describes a relaxation processes to the Fermi surface. We also use the dimensionless amplitude of velocity oscillations induced by a microwave field $\epsilon = e|\mathbf{E}|/(m\omega v_F)$. As in Ref. 9, in the following we use units with $v_F = 1$. The last two terms I_{ec} and I_s in (1) account for elastic collisions with the wall and small-angle scattering. Disorder scattering is modeled as random rotations of $\mathbf{v}$ by small angles in the interval $\pm\alpha_i$ with Poissonian distribution over time interval $\tau_i = 1/\omega$. The amplitude of noise is assumed to be relatively small so that the mean-free path ℓ_e is much larger than the cyclotron radius $r_c = v_F/\omega_c$. We note that the dissipative term is also known as a Gaussian thermostat[12] or as a Landau-Stuart dissipation.[10] The dynamical evolution described by Eq. (1) is simulated numerically using the Runge-Kutta method. Following Ref. 9 we call this system model (W1) [equivalent to model (1) in Ref. 9].

We note that for typical experimental ZRS parameters we have electron density $n_e = 3.5 \times 10^{11}$ cm^{-2}, effective electron mass $m = 0.065m_e$, microwave frequency $f = \omega/2\pi = 50$ GHz, and Fermi energy $E_F = mv_F^2/2 = \pi n_e\hbar^2/m = 0.01289$ V, corresponding to $E_F/k_B = 149.5$ K, with Fermi velocity $v_F = 2.641 \times 10^7$ cm/s. At such a frequency the cyclotron resonance $\omega = \omega_c = eB/mc$ takes place at $B = 0.1161$ T with the cyclotron radius $r_c = v_F/\omega_c = 0.8873$ μm. At such a magnetic field we have the energy spacing between Landau levels $\hbar\omega = \hbar\omega_c = 0.2067$ mV $= 2.40$ K $\times k_B$ corresponding to a Landau level $\nu = E_F/\hbar\omega_c \approx 62$. For a microwave field strength $E = 1$ V/cm we have the parameter $\epsilon = eE/(m\omega v_F) = 0.003261$. With these physical values of system parameters we can always recover the physical quantities from our dimensionless units with $m = e = v_F = 1$.

Examples of orbits running along the edge of specular wall are given in Ref. 9 (see Fig. 1 there). A microwave field creates resonances between the microwave frequency ω and a frequency of nonlinear oscillations of orbits colliding with the wall. Due to the specular nature of this collision the electron motion has high harmonics of cyclotron frequency that leads to the appearance of resonances around $j = 1,2,3,4,\ldots$ (there is an additional shift of approximate value $1/4$ to j_r values due to a finite width of nonlinear resonance).

To characterize the dynamical motion it is useful to construct the Poincaré section following the standard methods of nonlinear systems.[13,14] We consider the Hamiltonian case at $\gamma_0 = 0$ in the absence of noise. Also we choose a linear polarized microwave field being perpendicular to the wall which is going along the x axis (same geometry as in Ref. 9). In this case the generalized momentum $p_x = v_x + By = y_c$ is an integral of motion since there are no potential forces acting

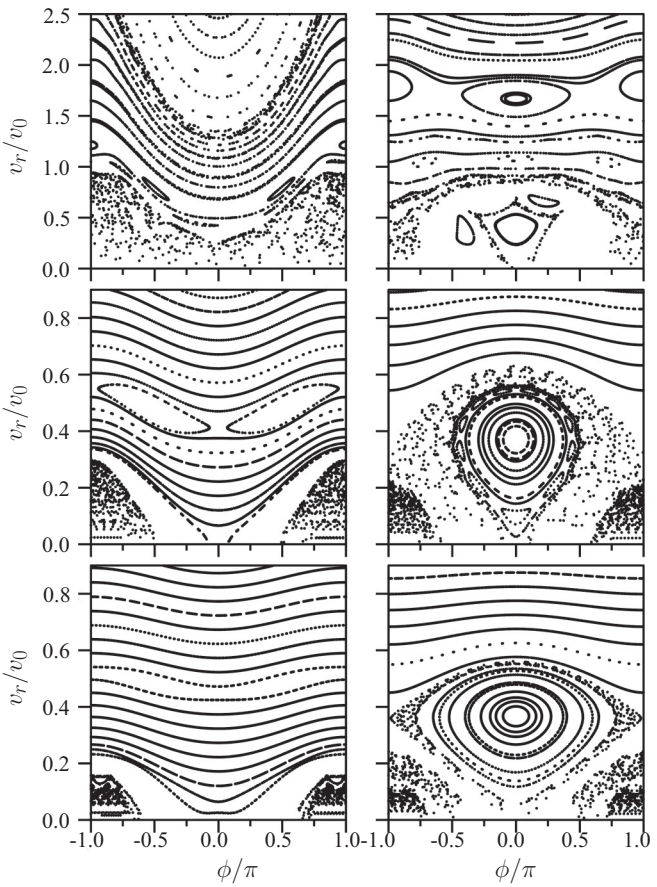

FIG. 1. Poincaré sections of Hamiltonian (2) for $j = 7/4$ (left column) and $j = 9/4$ (right column) and different amplitudes of microwave field $\epsilon = 0.02,0.04,0.2$ (from bottom to top). Here, the integral $p_x/mv_F = 1$, trajectories start from wall with fixed $v_x = p_x = v_0 = 1$. Data for model (W1) at $\gamma_0 = 0$, $\alpha_i = 0$.

on electrons along the wall (here we use the Landau gauge with a vector potential $A_x = By$). The momentum p_x determines a distance y_c between a cyclotron center and the wall, which also remains constant in time. The Hamiltonian of the system has the form

$$H = p_y^2/2 + (p_x - By)^2/2 + \epsilon\omega y \cos\omega t + V_w(y), \quad (2)$$

where $V_w(y)$ is the wall potential being zero or infinity for $y < 0$ or $y \geqslant 0$. Thus, we have here a so-called case of one and a half degrees of freedom (due to periodic dependence of the Hamiltonian on time) and the Poincaré section has continuous invariant curves in the integrable regions of phase space.[13,14]

The Poincaré sections for (1) and (2) at $j = 7/4, 9/4$ and various amplitudes of microwave field ϵ are shown in Fig. 1. It shows a velocity v_y at moments of collision with the wall at $y = 0$ as a function of microwave phase $\phi = \omega t$ at these moments of time. All orbits initially start at the wall edge $y = 0$ with the initial velocity $v_x = v_0 = p_x = y_c$. The value of $p_x = y_c$ is the integral of motion. However, the kinetic energy of electron $E_k = (v_x^2 + v_y^2)/2$ varies with time. We see that at a small $\epsilon = 0.02$ the main part of the phase space is covered by invariant curves corresponding to integrable dynamics. However, the presence of a chaotic component with scattered points is also visible in the vicinity of the separatrix of resonances, especially at large $\epsilon = 0.2$. The points at v_y close to zero correspond to orbits only slightly touching the wall, while the orbits at $v_y/v_0 \gg 1$ have a large cyclotron radius and collide with the wall almost perpendicularly. There are also sliding orbits which have the center of cyclotron orbit inside the wall ($y_c > 0$) but we do not discuss them here. Indeed, the orbits, which only slightly touch the wall ($y_c \approx -v_F/\omega_c$), play the most important role for transport since the scattering angles in the bulk are small for high-mobility samples and an exchange between bulk and edge goes via such type of dominant orbits.[9]

We note that the section of Fig. 1 at $j = 9/4$, $\epsilon = 0.02$ is in a good agreement with those shown in Fig. 1(b) of Ref. 9. However, here we have single invariant curves while in Ref. 9 the curves have a certain finite width. This happens due to the fact that in Ref. 9 the Poincaré section was done with trajectories having different values of the integral $p_x = y_c$ that gave some broadening of invariant curves. For a fixed integral value we have no overlap between invariant curves as is well seen in Fig. 1 here.

The phase space in Fig. 1 has a characteristic resonance at a certain v_y/v_0 value which position depends on j.[9] An approximate description of the electron dynamics and phase space structure can be obtained on a basis of the Chirikov standard map.[13–15] In this description developed in Ref. 9 an electron velocity has an oscillating component $\delta v_y = \epsilon \sin\omega t$ (assuming that $\omega > \omega_c$) and a collision with the wall gives a change of modulus of v_y by $2\delta v_y$ (like a collision with a moving wall). For small collision angles the time between collisions is $\Delta t = 2(\pi - v_y)/\omega_c$. Indeed, $2\pi/\omega_c$ is the cyclotron period. However, the time between collisions is slightly smaller by an amount $2v_y/\omega_c$: At $v_y \ll v_x \approx v_F$ an electron moves in an effective triangular well created by the Lorentz force and like for a stone thrown against a gravitational field this gives the above reduction of Δt (formally this expression for Δt is valid for sliding orbits but for orbits slightly touching the wall we have the same Δt but with minus that gives the correction $-2v_y/\omega_c$). The same result can be obtained via semiclassical quantization of edge states developed in Ref. 16. It also can be found from a geometric overlap between the wall and cyclotron circle. This yields an approximate dynamics description in terms of the Chirikov standard map:[13]

$$\bar{v}_y = v_y + 2\epsilon \sin\phi + I_{cc}, \quad \bar{\phi} = \phi + 2(\pi - \bar{v}_y/\rho)\omega_/\omega_c, \quad (3)$$

with the chaos parameter $K = 4\epsilon\omega/(\rho\omega_c)$. Usually we are in the integrable regime with $K < 1$ due to small values of ϵ used in experiments. A developed chaos appears at $K > 1$.[13,14] Here bars mark the new values of variables going from one collision to a next one, v_y is the velocity component perpendicular to the wall, and $\phi = \omega t$ is the microwave phase at the moment of collision. Here we introduced a dimensionless parameter ρ which is equal to $\rho = 1$ for the case of the wall model (W2) considered here. However, we will show that for the dynamics around a disk with a radial field in model (DR1) we have the same map (3) with $\rho = 1 + r_c/r_d$. Thus it is convenient to write all formulas with ρ. We note that a similar map (3) describes also a particle dynamics in a one-dimensional triangular well and a monochromatic field.[17]

The term $I_{cc} = -\gamma_c v_y + \alpha_n$ in (3) describes dissipation and noise. The latter gives fluctuations of velocity v_y at each iteration [$-\alpha < \alpha_n < \alpha$; corresponding to random rotation of velocity vector in (1)]. Damping from electron-phonon and electron-electron collisions contributes to γ_c. The Poincaré sections of this map are in good agreement with those obtained from the Hamiltonian dynamics as seen in Fig. 1 here and in Fig. 1 in Ref. 9. Following Ref. 9 we call this system model (W2) [equivalent to model (2) in Ref. 9].

A phase shift of ϕ by 2π does not affect the dynamics and thus the phase space structure changes periodically with integer values of j. Indeed, the position of the main resonance corresponds to a change of phase by an integer number of 2π values $\bar{\phi} - \phi = 2\pi m = 2(\pi - v_y/\rho)\omega/\omega_c$ that gives the position of resonance at $v_{\rm res} = v_y = \pi\rho(1 - m\omega_c/\omega) = \pi\rho\delta j/j$ where m is the nearest integer of ω/ω_c and δj is the fractional part of j. Due to this relation we have the different resonance position for $j = 7/4$ and $9/4$ being in agreement with the data of Fig. 1 at small values of ϵ when nonlinear corrections are small (we have here $\rho = 1$). Thus at $j = 9/4$ we have the resonance position at $v_y = 0.1111\pi \approx 0.35$ in agreement with Fig. 1 (right bottom panel). For $j = 2$ we have $v_y = 0$ and at $j = 7/4$ the resonance position moves to a negative value $v_y = -0.45$. Thus, at $j = 2; 7/4$ the resonance separatrix easily moves particles out from the edge at $v_y < 0$ where they escape to the bulk due to noise. In contrast at $j = 9/4$ particles move along the separatrix closer to the edge being then captured inside the resonance which gives synchronization of the cyclotron phase with the microwave phase. This mechanism stabilizes the transmission along the edge.

In Ref. 9 it is shown that the orbits started in the edge vicinity are strongly affected by a microwave field that leads to ZRS-type oscillations of transmission along the edge and longitudinal resistivity R_{xx}. The ZRS structure appears both in the frame of dynamics described by (1) [model (W1)] and in map description (3) [model (W2)]. The physical mechanism is based on synchronization of a cyclotron phase with a phase

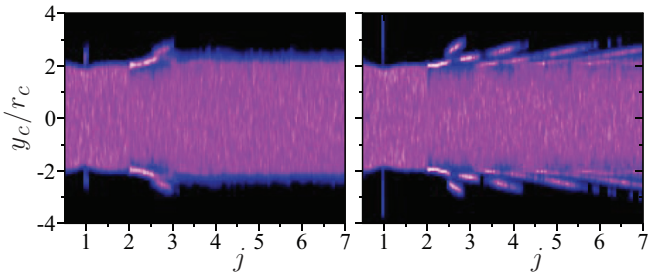

FIG. 2. (Color online) Density distribution w of electrons as a function of their dimensionless cyclotron center position y_c/r_c between two walls and the frequency ratio $j = \omega/\omega_c$. The distance between specular walls is $6r_c$. The amplitude of microwave field is $\epsilon = 0.1$ with polarization parallel (left panel) and perpendicular (right panel) to the walls (see text for more details). Here $\gamma_0/\omega = 0.05$, $\alpha_i = 0.01$, $\tau_i = 1/\omega$. The variation of $j = \omega/\omega_c$ is obtained by changing magnetic field ($\omega_c = B$) keeping $\omega = \text{const.}$; 100 electrons are simulated at each j up to time $t_r = 10^5/\omega$. Density is proportional to color changing from zero (black) to maximal density (white). Data for model (W1).

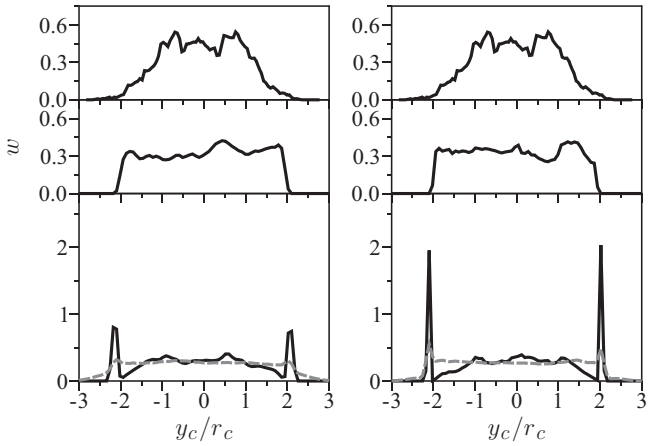

FIG. 3. Profile of density distribution $w(y_c)$ as a function of y_c/r_c for microwave polarization parallel (left panels) and perpendicular (right panels) to the walls. Here we have no microwave at top panels, $\epsilon = 0.1$, $j = 1.7$ at middle panels, $\epsilon = 0.1$, $j = 2.4$ at bottom panels. In all panels we have noise amplitude $\alpha_i = 0.01$ as in Fig. 2; dashed curves in bottom panels are obtained with $\alpha_i = 0.05$. Simulations are done with 500 trajectories, other parameters are the same as in Fig. 2. Data for model (W1).

of microwave driving that leads to stabilization of electron transport along the edge. An extensive amount of numerical data has been presented in Ref. 9 and we think there is no need to add more. Here, we simply want to illustrate that even those orbits which start in the bulk are affected by this synchronization effect. For that we take a band of two walls with a bandwidth between them being $\Delta y = L = 6r_c$. Initially 100 trajectories are distributed randomly in a bulk part between walls when a cyclotron radius is not touching the walls ($-2r_c < y_c < 2r_c$). Their dynamics is followed during the run time $t_r = 10^5/\omega$ according to Eq. (1) and a density distribution $w(y_c)$ averaged in a time interval $5 \times 10^4 < \omega t < 10^5$ is obtained for a range of $0.5 \leqslant j \leqslant 7$ (261 values of j are taken homogeneously in this interval). The value of t_r approximately corresponds to a distance propagation along the wall of $r_w \sim v_y t_r \sim 0.1 v_F t_r \sim 5 \times 10^3 v_F/\omega \sim 0.2$ cm at typical values $v_F \sim 2 \times 10^7$ cm/s, $\omega/2\pi = 100$ GHz. This is comparable with a usual sample size used in experiments.[1,2] Similar values of r_w were used in Ref. 9.

The dependence of density w on y_c and j is shown in Fig. 2 for two polarizations of the microwave field. The data show that orbits from a bulk can be captured in the edge vicinity for a long time giving an increase of density in the vicinity of the edge. This capture is significant around resonance values $j \approx j_r$. This is confirmed by a direct comparison of density profiles in Fig. 3 at $j = 1.7 \approx 2 - 1/4$ and $j = 2.4 \approx 2 + 1/4$. In the latter case we have a large density peak due to trajectories trapped in a resonance (see Fig. 1) where they are synchronized with the microwave field. An increase of noise amplitude α_i gives a significant reduction of the amplitude of these resonant peaks (Fig. 3, bottom panels). The increase of density is more pronounced for polarization perpendicular to the wall in agreement with data shown in Fig. 2 of Ref. 9.

The results of Figs. 2 and 3 clearly show that the electrons from the bulk can be trapped by a microwave field in an edge vicinity that enhances the propagation along the edge. At the same time the skipping orbits, the cyclotron circle center of which is outside the sample, are practically unaffected by a microwave field (indeed, from Fig. 3 we see a significant density drop at the edge vicinity that results from a separation of skipping orbits from those linked with the bulk). Such orbits remain disconnected from the bulk and hence they do not give significant contribution to R_{xx} as is the case in absence of microwave field.

We also performed numerical simulations using Eq. (1) with a smooth wall modeled by a potential $V_w(y) = \kappa y^2/2$. For large values κ/ω_c (e.g., $\kappa/\omega_c = 10$) we find the Poincaré sections to be rather similar to those shown in Fig. 1 that gives a similar structure of electron density as in Figs. 2 and 3. A finite wall rigidity can produce a certain shift of optimal capture conditions appearing as a result of additional correction to a cyclotron period due to a part of orbit inside the wall.

The data presented in this section show that electrons from the bulk part of the sample can be captured for a long time in the edge vicinity thereby increasing the electron density near the edge. This effect is very similar to the accumulation of electrons on the edges of the electron cloud under ZRS conditions that was reported for surface electrons on helium in Ref. 7. However we have to emphasize that the confinement potential for surface electrons is very different from the hard wall potential assumed in our simulations; as a consequence our results cannot be applied directly to this case. It is possible that the formation of ballistic channels on the edge of the sample combined with the redistribution of the electron density can effectively short the bulk contribution and induce directly a vanishing R_{xx}. However, it is also very important to understand how a scattering on impurities inside the bulk is affected by a microwave radiation. Indeed, the volume of the bulk is significantly larger than the volume of strips of cyclotron radius width along the edges. Thus a presence of low-density sharp impurity scatterers inside the bulk can give the dominant contribution to the global resistivity of a large-size sample.

Hence, the analysis of scattering inside the bulk is very important. We study this question in the next sections.

III. SCATTERING ON A SINGLE DISK

It should be noted that resistivity properties of a regular lattice of disk antidots in 2DEG have been studied experimentally[18,19] and theoretically.[20,21] But the effects of the microwave field were not considered till present.

In our studies we model an impurity as a rigid disk of fixed radius r_d; we measure r_d in units of distance v_F/ω, keeping $\omega =$ constant and changing $\omega_c = B$. We usually have a fixed ratio $r_d\omega/v_F = 1$. In a magnetic field a cyclotron radius moves in free space only due to a static dc electric field E_{dc}. We fix the direction of E_{dc} along the x axis and measure its strength by a dimensionless parameter $\epsilon_s = E_{dc}/(\omega v_F)$. Even in the absence of a microwave field a motion in the vicinity of the disk in crossed static electric and magnetic fields of moderate strength is not so simple. The studies presented in Refs. 22 and 23 show that dynamics in the disk vicinity is described by a symplectic disk map which is rather similar to the map (3). It is characterized by a chaos parameter $\epsilon_d = 2\pi v_d/(r_d\omega_c)$ where $v_d = E_{dc}/B$ is the drift velocity; ϵ_d gives an amplitude of change of radial velocity at collision. Orbits from the vicinity of the disk can escape for $\epsilon_d > 0.45$.[22]

We start our analysis from the construction of the Poincaré section in the presence of the microwave field at zero static field. To have a case with one and half degrees of freedom we start from a model case when the microwave field is directed only along the radius from the disk center. The dynamics is described by Eq. (1) with a dimensionless microwave amplitude ϵ. The dynamical evolution is obtained numerically by the Runge-Kutta method. At first we consider a case without dissipation and noise. Due to radial force direction the orbital momentum is an additional integral of motion (as $p_x = y_c$ for the wall case) and thus we have again 3/2 degrees of freedom. We call this disk model with radial microwave field as model (DR1).

The Poincaré sections at the moments of collisions with the disk are shown in Figs. 4 and 5 for model (DR1). Here, v_r is the radial component of electron velocity and ϕ is a microwave phase both taken at the moment of collision with the disk. We see that the phase space structure remains approximately the same when j is increased by unity (compare $j = 9/4, 13/4$ panels in Fig. 4). This happens for orbits only slightly touching the disk (small v_r) since the microwave phase change during a cyclotron period is shifted by an integer amount of 2π (in a first approximation at $r_d \ll r_c$). The similarity between the wall and disk cases is directly seen from Fig. 5 as well as periodicity with $j \to j + 1$.

In fact in the case of a disk with a radial field the dynamics can be also described by the Chirikov standard map (3) where v_y should be understood as a radial velocity v_r at the moment of collision. The second equation has the same form since the change of the phase between two collisions is given by the same equation but with the parameter $\rho = 1 + r_c/r_d$. This expression for ρ is obtained from the geometry of slightly intersecting circles of radius r_d for disk and radius r_c for cyclotron orbit (the angle segment of the cyclotron circle is $\Delta\varphi = 2v_r/\rho$). For $r_d \gg r_c$ this expression naturally reproduces the wall case

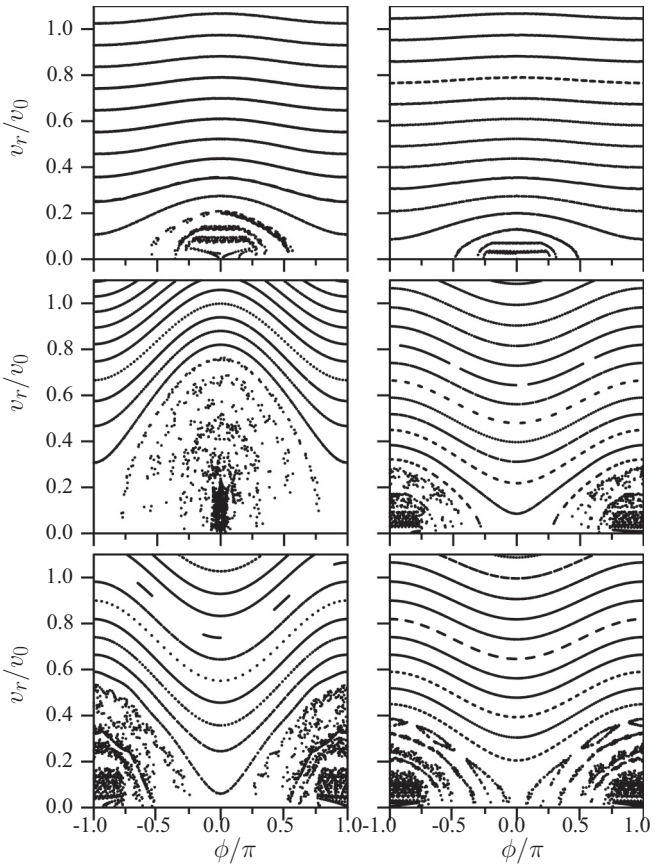

FIG. 4. Poincaré section for Hamiltonian dynamics in a disk vicinity in presence of radial microwave field. Left column panels: $j = 7/4, 2, 9/4$ at $\epsilon = 0.04$ (from top to bottom); right column panels: $j = 7/4, 13/4, 9/4$ at $\epsilon = 0.02$. Here the integral of orbital momentum is $\ell_0/v_F r_d = v_0/v_F = 1$, trajectories start from disk with fixed tangent velocity component $v_0 = 1$. Data for model (DR1).

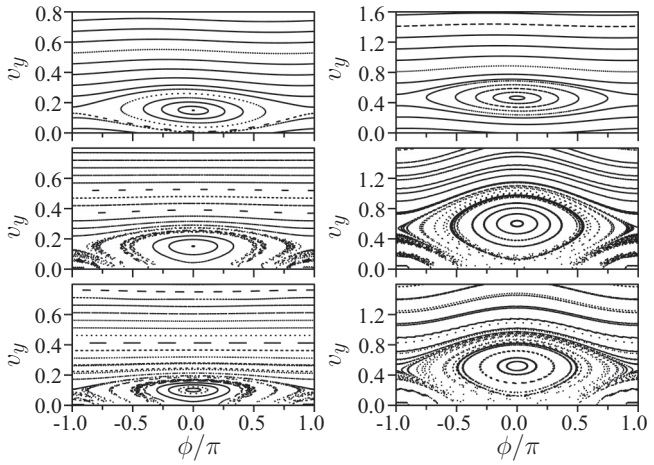

FIG. 5. Poincaré sections for wall model (W1) (left) and disk model with radial electric field (DR1) (right) at $\epsilon = 0.01$ and $j = 2.1$ (top, middle) and $j = 3.1$ (bottom). Top panels are obtained from the Chirikov standard map (3) at $\rho = 1$ (left top panel), corresponding to the wall model (W2), and at $\rho = 1 + j = 3.1$ (right top panel), corresponding to the disk model (DR2). Middle and bottom panels are obtained from solution of Newton equations (1) for wall (left) and disk (right). Other parameters are as in Fig. 1 and Fig. 4; v_y and v_r are expressed in units of v_F. There is no dissipation and no noise.

while at $r_d \ll r_c$ we have the correction term proportional to $\bar{v}_y$ going to zero that also well corresponds to the geometry of two disks. After such modification of ρ we find that the resonance positions $v_{\rm res} = \pi\rho\delta j/j$ are proportional to ρ. Thus the model (DR1) reduced to the map description (3) at $\rho > 1$ is called model (DR2).

The expression for $v_{\rm res}$ works rather well. Indeed, for $j = 2.1$ in Fig. 5 we obtain $v_{\rm res} = 0.149$ for model (W2) and 0.463 for model (DR2). These values are in a good agreement with numerical values $v_{\rm res} \approx 0.15$ for model (W2) and $v_{\rm res} \approx 0.6$ for model (DR1). In the latter case the agreement is less accurate due to a larger size of nonlinear resonance. The comparison of Poincaré sections given by the Chirikov standard map (3) and the dynamics from Newton equations, shown in Fig. 5, confirm the validity of the map description.

According to the well-established results for the Chirikov standard map[13] we find for models (W1), (W2) and (DR1), (DR2) the width of separatrix δv and the corresponding resonance energy width $E_r = (\delta v)^2/2$:

$$\begin{aligned} E_r &= 16\epsilon\omega_c\rho E_F/\omega, \quad \rho = 1 + r_c/r_d, \\ v_{\rm res} &= \pi\rho\delta j/j, \quad \delta v = 4\sqrt{\epsilon\rho/j}, \\ \delta j_\epsilon &= \delta v j/(2\pi\rho), \quad j = \omega/\omega_c, \end{aligned} \tag{4}$$

where δj_ϵ is the resonance shift produced by a resonance half width $\delta v/2 = v_{\rm res}$. This relation shows that for the disk case this energy is increased by a factor ρ compared to the wall case. In the majority of our numerical simulations we have $\rho = 1 + j$.

Thus the radial field models (DR1), (DR2) represent a useful approximation to understand the properties of dynamics in the disk vicinity, but a real situation corresponds to a linear microwave polarization and the Poincaré section analysis should be modified to understand the dynamics in this case.

Therefore we start to analyze the scattering problem on a disk in the presence of weak static field ϵ_s and microwave field ϵ using Eq. (1). For the scattering problem we find it more simple to have dissipation work only at the time moments of electron collisions with disk: At such time moments the modulus of electron velocity is reduced by a factor $|v| \to |v|/(1 + \gamma_d)$; the reduction is done only if the kinetic energy of the electrons is larger than the Fermi energy. Such a dissipation can be induced by phonon excitations inside the antidot disk. We fix the geometry directing the dc field along the x axis and microwaves along the y axis. The noise is modeled in the same way as above in Eq. (1). We call this system disk model (D1). Below we present data for a fixed value of $\gamma_d = 0.01$ but we checked that the variation of this parameter by a factor 2–3 does not modify the typical dependence $R_{xx}(j)$ presented below.

We note that the presence of dissipation only in the vicinity of the disk corresponds to the experimental reality: The ZRS effect exists only in high-mobility samples; in a free space without disks we have only a small smooth angle scattering which cannot generate $j > 1$ resonances due to the absence of such matrix elements in an oscillator potential effectively created by a magnetic field. Therefore the dissipative processes give significant contribution to transport only in the vicinity of sharp impurities (disks) or sample edges.

Examples of electron cyclotron trajectories scattering on a disk are shown in Fig. 6. In the absence of the microwave field

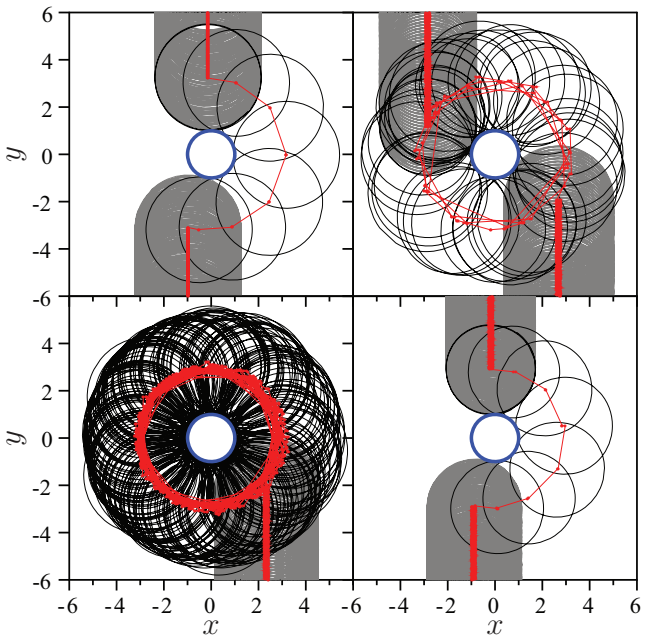

FIG. 6. (Color online) Scattering of electron cyclotron trajectory on a disk scatterer (blue/black circle) in model (D1). Top left panel shows the case in absence of microwave, $\epsilon = 0$, $j = 9/4$. Top right panel: Temporary captured path at $\epsilon = 0.04$, $j = 9/4$. Bottom left panel: Path captured forever at $\epsilon = 0.04$, $j = 9/4$. Bottom right panel: No capture at $\epsilon = 0.04$, $j = 2$. The trajectory part colliding with disk is shown by black curve; its part before and after collisions is shown in gray. The red (light gray) points and curves show the trajectory of cyclotron center. Here the dissipation parameter is $\gamma_d = 0.01$; the static electric field is directed along the x axis and $\epsilon_s = 0.001$; the microwave field is directed along the y axis. There is no noise here. Coordinates x, y are expressed in units of r_d. Data for model (D1).

a trajectory escapes from the disk rather rapidly. A similar situation appears at $j = 2$ and a microwave field with $\epsilon = 0.04$. In contrast, for $j = 9/4$ and $\epsilon = 0.04$ a trajectory can be captured for a long time or even forever depending on the initial impact parameter.

For some impact parameters a trajectory can be captured for a very long time t_c; in certain cases in the absence of noise we have $t_c = \infty$. At such long capture times the collisions with the disk become synchronized with the phase ϕ of the microwave field at the moment of collisions. This is directly illustrated in Fig. 7 where we show the angle θ of a collision point on the disk, counted from the x axis, in dependence on ϕ. Indeed, the dependence θ on ϕ forms a smooth curve corresponding to synchronization of two phases. At the same time the radial velocity at collisions v_r moves along some smooth invariant curve $v_r(\phi)$ in the phase space (v_r, ϕ). However, to make a correct comparison with the radial field models (DR1), (DR2) we should take into account that the cyclotron circle rotates around the disk so that we should draw the Poincaré section in the rotational phase $\phi' = \phi - \theta$. In this representation we see the appearance of the resonance (see right column of Fig. 7) that is similar to that seen in Figs. 4 and 5 for the radial field models.

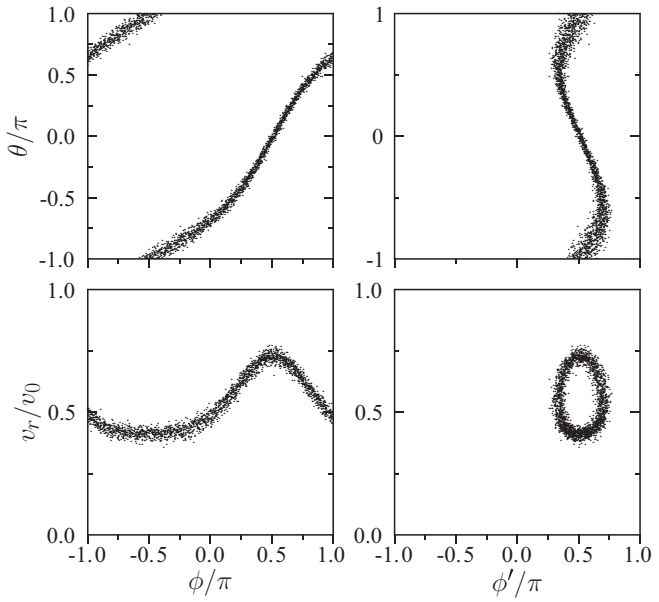

FIG. 7. Synchronization between disk collision angle θ and microwave phase ϕ. Left column: Dependence of angle θ of collision point on disk, counted from x axis, and radial velocity v_r, taken at collision, on microwave phase ϕ. Right column: Same as in left column with $\phi' = \phi - \theta$. Here $j = 2.25$, $\epsilon = 0.04$, $\epsilon_s = 0.001$, $\gamma_d = 0.01$, $v_0 = v_F$, there is no noise; points are shown for times $10^4/\omega < t < 10^5/\omega$, the capture time of this orbit is $t_c > 10^5/\omega$. Data for model (D1).

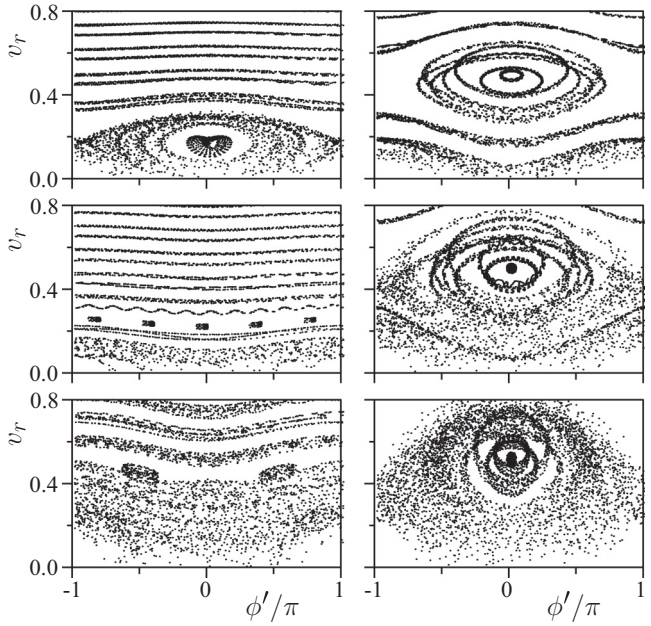

FIG. 8. Poincaré sections in phase plane (v_r,ϕ') with $\phi' = \phi - \theta$ for $j = 2.1$, $\epsilon = 0.01$ (left top); $j = 2.25$, $\epsilon = 0.01$ (right top); $j = 2.75$, $\epsilon = 0.02$ (left middle); $j = 2.25$, $\epsilon = 0.02$ (right middle); $j = 2.75$, $\epsilon = 0.04$ (left bottom); $j = 2.25$, $\epsilon = 0.04$ (right bottom); v_r is expressed in units of v_F. Data for model (D1), no noise no dissipation.

A more direct correspondence between radial field models (DR1), (DR2) and model (D1) with a linearly polarized microwave field is well seen from the Poincaré sections shown in the rotation frame of phase $\phi' = \phi - \theta$ in Fig. 8. In this frame we see directly the resonance at $j = 2.1, 2.25$ being very similar to the wall case and the radial field model. However, the positions of resonance at $v_r = v_{\rm res}$ are different from those in Fig. 5. Of course in the rotation frame the orbital momentum is only approximately conserved that gives a broadening of invariant curves in Fig. 8.

We explain this as follows. For the linear polarized field of model (D1) the radial component of the microwave field is proportional to $\epsilon_r \sim \epsilon \sin\theta \cos\omega t \sim 0.5\epsilon \sin(\omega t - \theta)$ where we kept only the slow frequency component of the radial field [the neglected term with $\sin(\omega t + \theta)$ gives resonant values $v_{\rm res} > v_F$]. The radial field ϵ_r gives kicks to the radial velocity component at collisions with the disk similar to the case of model (DR2) described by Eq. (3): $\bar{v}_r = v_r + 0.5\epsilon \sin\phi'$, $\bar{\phi}' = \phi' + (2\pi j - 2\bar{v}_r j/\rho) - 2\bar{v}_r(\rho - 1)/\rho$. Here we use the radial field component phase $\phi' = \omega t - \theta$ at a moment of collision with the disk (the tangent component does not change v_r and can be neglected). The phase variation $\bar{\phi}' - \phi'$ has the first term $2\pi j - 2\bar{v}_r j/\rho$ being the same as for the radial field model (DR2), and an additional term related to rotation around the disk with $-\Delta\theta = -2\bar{v}_r(\rho - 1)/\rho$ which comes from geometry. Indeed, the segment angles of intersections of circles r_d and r_c are as follows: For disk radius r_d it is $\Delta\theta = 2\bar{v}_r(\rho - 1)/\rho$ and for cyclotron radius r_c it is $\Delta\varphi = 2\bar{v}_r/\rho$. Thus, their ratio is $\Delta\theta/\Delta\varphi = r_c/r_d$ in agreement with the geometrical scaling. This result can be obtained from the expression for $\Delta\varphi$ by interchange of two disks that gives the above expression for $\Delta\theta$ [at $r_d = r_c$ both shifts $\Delta\varphi = 2\bar{v}_r/\rho$ and $\Delta\theta = 2\bar{v}_r(\rho - 1)/\rho$ are equal].

Thus again the dynamical description is reduced down to the Chirikov standard map with slightly modified parameters giving us for the model (D1) the chaos parameter $K = 2\epsilon(j + \rho - 1)/\rho$ being usually smaller than unity, resonance position $v_{\rm res}$, resonance width δv, and the resonance energy width $E_r = (\delta v)^2/2$:

$$E_r = 8\epsilon\rho E_F/(\rho + j - 1), \quad \rho = 1 + r_c/r_d,$$
$$v_{\rm res} = \pi\rho\delta j/(j + \rho - 1), \quad \delta v = 4\sqrt{\epsilon\rho/(2(j + \rho - 1))},$$
$$\delta j_\epsilon = \delta v(\rho + j - 1)/(2\pi\rho), \; j = \omega/\omega_c, \qquad (5)$$

where δj_ϵ is a shift of resonance produced by a finite separatrix half width $\delta v/2$. For our numerical simulations we have $\rho = 1 + j$ with $v_{\rm res} = \pi(j + 1)\delta j/(2j)$, $\delta v = 2\sqrt{\epsilon(j + 1)/j}$, and $\delta j_\epsilon = (2/\pi)\sqrt{\epsilon j/(j + 1)}$.

At $\rho = j + 1$ Eq. (5) gives the values $v_{\rm res} = 0.232$ at $j = 2.1$ while the numerical data of Fig. 8 give $v_{\rm res} \approx 0.2$, and we have at $j = 2.25$ the theory value $v_{\rm res} = 0.567$ being in good agreement with the numerical value $v_{\rm res} \approx 0.5$ of Fig. 8. For $j = 2.75$ we have the resonance position at $v_r < 0$ corresponding to the bulk and thus the resonance is absent. The resonance width in Fig. 8 at $j = 2.25$, $\epsilon = 0.01$ can be estimated as $\delta v \approx 0.3$ that is in satisfactory agreement with the theoretical value $\delta v = 0.24$ from (5). We recall that in model (D1) we have only approximate conservation of orbital momentum that gives a broadening of invariant curves and makes determination of the resonance width less accurate. In spite of this broadening we see that the resonance description by the Chirikov standard map works rather well.

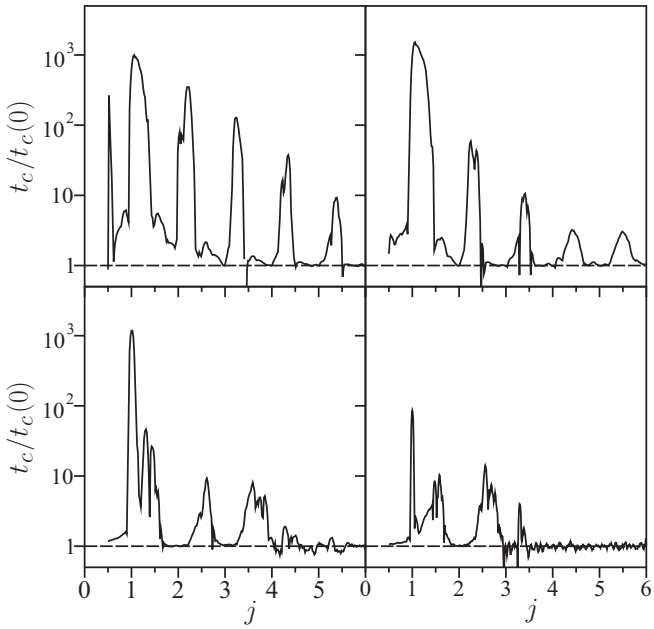

FIG. 9. Dependence of rescaled capture time $t_c/t_c(0)$ on j at $\epsilon = 0.04$ shown at various static fields: $\epsilon_s = 2.5 \times 10^{-4}$ (top left), 10^{-3} (top right), 8×10^{-3} (bottom left), 0.016 (bottom right). Here $\gamma_d = 0.01$, there is no noise. Data for model (D1).

In Fig. 9 we show the dependence of average capture time t_c on j in model (D1). The averaging is done over $N_s = 500$ trajectories scattered on the disk at all such impact parameters at which the cyclotron orbit can touch the disk. Here, we show the ratio $t_c/t_c(0)$ where $t_c(0)$ is an average capture time in the absence of microwaves. According to our numerical data we have an approximate dependence $\omega t_c(0) \approx 3/\sqrt{\epsilon_s}$ corresponding to a period of nonlinear oscillations in disk map description discussed in Refs. 22 and 23.

The data of Fig. 9 show a clear periodic dependence of capture time t_c on j corresponding to the periodicity variation of the Poincaré section with j (see Figs. 4, 5, and 8). This structure is especially visible at weak static fields. With an increase of ϵ_s this structure is suppressed. Indeed, at large ϵ_s even without microwave field the trajectories can escape from the disk as discussed in Refs. 22 and 22 and the microwave field does not affect the scattering in this regime.

The distributions of capture times are shown in Fig. 10. We clearly see that at resonant values of j a microwave field leads to the appearance of long capture times. For example, we have the probability to be captured for $t_c > 180/\omega$ being $W = 0.46$ at $j = 2.25$ while at $j = 2$ we have $W = 0$ (left panel in Fig. 10); and we have $W = 0.38$ at $j = 2.37$ while at $j = 1.9$ we have $W < 3 \times 10^{-4}$ (right panel in Fig. 10). These data confirm much stronger capture at certain resonant values of j.

The data of Figs. 9, 10 show that the scattering process on the disk is strongly modified by the microwave field. However, to determine the conductivity properties of a sample we need to know what is an average displacement Δx along the static field after a scattering on a single disk. Indeed, in our model a dissipation is present only during collisions with disk while in free space between disks the dynamics is integrable and

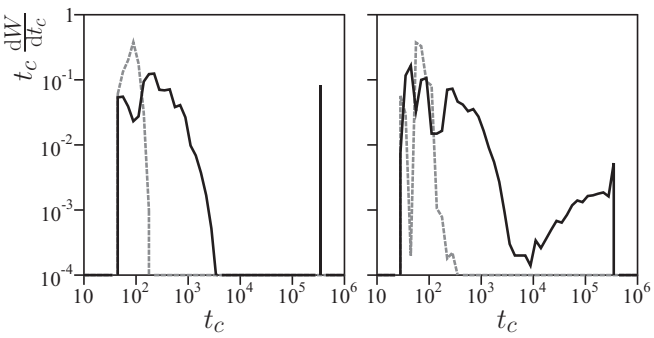

FIG. 10. Differential probability distribution $t_c dW/dt_c$ of capture times t_c for parameters of Fig. 9. Left panel: $j = 2$ (dashed curve for minimum of capturing probability) and $j = 2.25$ (full curve at maximum of capturing probability) at $\epsilon_s = 0.001$. Right panel: Similar cases at $j = 1.9$ (dashed curve) and $j = 2.37$ (full curve) at $\epsilon_s = 0.002$. Data are obtained with $N_s = 5 \times 10^4$ trajectories started at different impact parameters and running up to time $t = 3 \times 10^5/\omega$. Here t_c is expressed in units of $1/\omega$. Data for model (D1).

Hamiltonian. Hence during such a free space motion there is no displacement along the static field (the dissipative part of conductivity or resistivity appears only due to dissipation on the disk). The dependence of Δx on j is shown in Fig. 11. In the absence of microwave field at $\epsilon = 0$ we find $\Delta x \propto 1/j \propto B$ that corresponds to a simple estimate $\Delta x \propto \omega_c \gamma_d$. Indeed, without dissipation the system is Hamiltonian and hence there is no dissipative average displacement so that $\Delta x = 0$. The dissipation acts only at the collisions with the disk so that the displacement is proportional both to γ_d and the frequency of collisions with disk, which is proportional to $\omega_c \propto B$, thus leading to the above estimate.

The numerical data show that Δx is practically independent of ϵ_s and that $\Delta x = 0$ in absence of dissipation at $\gamma_d = 0$. In the presence of the microwave field we see that the displacement along the static field has strong periodic oscillations with j. The striking feature of Fig. 11 is the appearance of

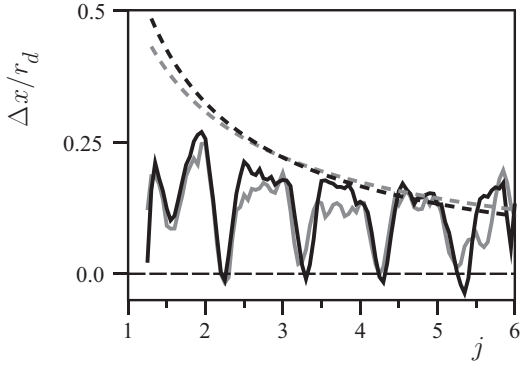

FIG. 11. Average shift Δx along static field after scattering on a single disk shown as a function of j at various amplitudes of static and microwave fields: $\epsilon_s = 0.0005$, $\epsilon = 0$ (gray dashed curve); $\epsilon_s = 0.001$, $\epsilon = 0$ (black dashed curve); $\epsilon_s = 0.0005$, $\epsilon = 0.04$ (gray full curve); $\epsilon_s = 0.001$, $\epsilon = 0.04$ (black full curve). The data are obtained by averaging over $N_s = 5 \times 10^3$ scattered trajectories with random impact parameters; here $\gamma_d = 0.01$, noise amplitude $\alpha_i = 0.005$. Data for model (D1).

windows of zero displacement $\Delta x \approx 0$ at resonance values $j_r = 9/4, 13/4, 17/4, \ldots$. We discuss how this scattering on a single disk modifies the resistance of a sample with a large number of disks in the next section.

IV. RESISTANCE OF SAMPLES WITH MANY DISKS

To determine a resistance of a sample with many disks we use the following scattering disk model. The scattering on a single disk in a static electric field ϵ_s is computed as described in the previous section with a random impact parameter inside the collision cross section $\sigma_d = 2(r_c + r_d)$. After that a trajectory evolves along the y axis according to the exact solution of Hamiltonian Eq. (1) (no dissipation and no noise) up to a collision with the next disk which is taken randomly on a distance between $2(r_c + r_d)$ and $2\ell_e$ where $\ell_e = 1/(\sigma_d n_d)$ is a mean-free path along the y axis and n_d is a two-dimensional density of disks [of course $\ell_e \gg 2(r_c + r_d)$]. In the vicinity of the disk the dynamical evolution is obtained with the Runge-Kutta solution of dynamical equations as was the case in the previous section. We use a low disk density with $n_d r_d^2 \sim 1/100$. The collision with the disk is done with a random impact parameter on the x axis of the disk vicinity: The impact parameter is taken randomly in the interval $[-(r_c + r_d),(r_c + r_d)]$ around disk center. Noise acts only when a center of cyclotron radius of trajectory is on a distance $r < r_d + r_c$ from disk center so that a collision with the disk is possible. After scattering on a disk a free propagation follows up to the next collision with a disk.

Along such a trajectory we compute the average displacement δx and δy after a time interval δt. In this way the number of collisions with disks is $N_{\rm col} \approx \delta y/\ell_e$ and a total displacement on the x axis is $\delta x \approx N_c \Delta x$ where Δx is the average displacement on one disk discussed in the previous section. We compute the global displacements $\delta x, \delta y$ on a time interval $\delta t = 10^6/\omega$ averaging data over 200 trajectories. We call this system model (D2).

We stress that in the model D2 we take into account exactly scattering on all disks in the sample, small-angle scattering in the vicinity of the disks. However, for efficiency of numerical simulations we neglect small-angle scattering in the free space between disks. We argue that small-angle scattering in free space cannot generate dips at high $j > 1$ since the corresponding dipole matrix elements are absent in the Hamiltonian of the linear oscillator. Also the ZRS effect exists only in high-mobility samples and hence a contribution to conductivity from a free space with small-angle scattering is small and it cannot add a significant constant background to conductivity (or resistivity) in the ZRS phase. However, small-angle scattering plays an important role in the vicinity of the edge or disk where it is exactly taken into account in our numerical modeling. If the free space contains smooth potential variations on a length which is significantly larger than a cyclotron radius then the high $j > 1$ harmonics are exponentially small due to the adiabatic theorem and analyticity of motion. Small delta-function-type defects in a space between disks can generate high j harmonics but their amplitude is small in the case of small-amplitude scattering on defects with a small potential amplitude. In the case of strong defects we come to a situation being similar to the case of disk scattering which we analyze here in detail. The defects with size being smaller than a magnetic length should be treated in the frame of quantum scattering which we discuss in Sec. VII.

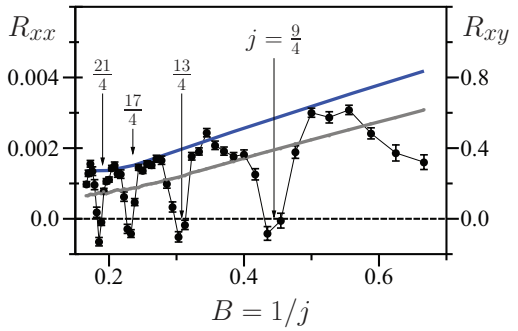

FIG. 12. (Color online) Dependence of resistivity R_{xx} and R_{xy} on magnetic field $B = 1/j$ (resistivity is expressed in arbitrary numerical units). Blue and gray curves show respectively R_{xx} and R_{xy} in absence of microwave field. Black curve with points shows R_{xx} dependence of B at microwave field $\epsilon = 0.04$ (here B is expressed in units of $1/\omega = \text{const.}$). Here $\epsilon_s = 0.001$, $\gamma_d = 0.01$, noise amplitude $\alpha_i = 0.005$, $\tau_i = 1/\omega$. Resonant values j_r are shown by arrows; bars show statistical errors for R_{xx}. Data are obtained by averaging over 200 trajectories propagating up to time $t = 10^6/\omega$. Data for model (D2).

Thus the current components are equal to $j_x = \delta x/\delta t$, $j_y = \delta y/\delta t$ and conductivity components are $\sigma_{xx} = j_x/E_{dc}$, $\sigma_{xy} = j_y/E_{dc}$ (the current is computed per one electron). We work in the regime of the weak dc field where j_x, j_y scales linearly with E_{dc}. The current j_y is determined by the drift velocity $v_d = E_{dc}/B \ll v_F$. Since the mean-free path is large compared to disk size $\ell_e \gg r_c \geqslant r_d$ we have an approximate relation $\sigma_{xy} \approx 1/B$, $\sigma_{xx} \approx \Delta x/B\ell_e \approx \sigma_{xy}\Delta x/\ell_e$. As in 2DEG experiments[1,2] we have in our simulations $\sigma_{xy}/\sigma_{xx} = R_{xy}/R_{xx} \sim 100$ (see Fig. 12). The resistivity is obtained by the usual inversion of conductivity tensor with $R_{xx} = \sigma_{xx}/(\sigma_{xx}^2 + \sigma_{xy}^2) \approx \sigma_{xx}/\sigma_{xy}^2$, $R_{xy} = \sigma_{xy}/(\sigma_{xx}^2 + \sigma_{xy}^2) \approx 1/\sigma_{xy}$. The dependence of R_{xx}, R_{xy}, expressed in arbitrary numerical units, on magnetic field $B = \omega/j = 1/j$ is shown in Fig. 12.

In the absence of microwave field we find $R_{xy} \propto B$ and $R_{xy}/R_{xx} \approx 200$ similar to experiments.[1,2] For small noise amplitude (e.g., $\alpha_i = 0.005$) we have R_{xx} growing linearly with B (see Fig. 12) but at larger amplitudes (e.g., $\alpha_i = 0.02$) its increase with B becomes practically flat showing only 30% increase in a given range of B variation.

In the presence of a microwave field the dependence of R_{xx} on B is characterized by periodic oscillations with minimal R_{xx} values being close to zero at resonant values of $j = j_r$ well visible in Fig. 12. The dependence of R_{xx}, R_{xy} rescaled to their values $R_{xx}(0)$, $R_{xy}(0)$ in the absence of microwave field is shown in Fig. 13 at various amplitudes of noise and fixed ϵ, and in Fig. 14 at various ϵ and fixed noise amplitude α_i. We see that increase of noise leads to an increase of minimal values of R_{xx} at resonant values j_r. In a similar way a decrease of microwave power leads to increase of minimal values of R_{xx} at j_r. At the same time the Hall resistance R_{xy} is only weakly affected by microwave radiation as also happens in ZRS experiments.

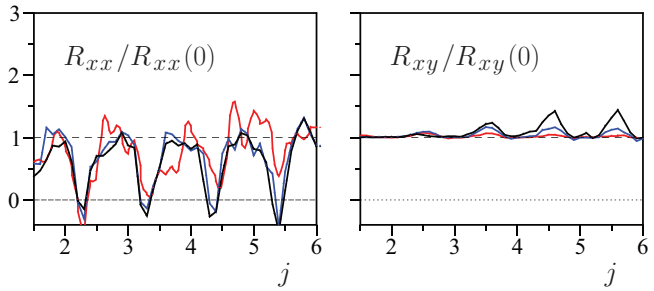

FIG. 13. (Color online) Rescaled values of resistivity R_{xx} (left panel) and R_{xy} (right panel) as function of $j = \omega/\omega_c$ at various noise amplitudes $\alpha_i = 0.005$ (black curve), 0.01 (blue/dark curve), 0.02 (red/gray curve). Here $\epsilon = 0.04$, $\epsilon_s = 0.001$, other parameters are as in Fig. 12. Curves are drawn though numerical points obtained with a step $\Delta j = 0.1$. Data for model (D2).

These results are in qualitative agreement with the ZRS experiments. On the basis of our numerical studies we attribute the appearance of approximately zero resistance at j_r values in our bulk model of disk scatterers to long capture times of orbits in disk vicinity at these j_r values (see Fig. 9). During this time t_c noise gives fluctuations of collisional phase θ and due to that a cyclotron circle escapes from the disk practically at random displacement Δx that after averaging gives average $\Delta x = 0$. Since resistivity is determined by the average value of Δx this leads to appearance of ZRS. We note that this mechanism is different from the one of edge transport stabilization discussed here and in Ref. 9. However, both mechanisms are related to a long capture times near the edge or near the disk that happens due to synchronization of the cyclotron phase with microwave field phase and capture inside the nonlinear resonance.

To illustrate the capture inside the resonance we present the distributions of trajectories from Fig. 14 shown in the phase space plane (v_r,ϕ') at the moments of collisions with disks in Fig. 15. This is similar to the Poincaré sections of Fig. 8. However, now we consider the real case of diffusion and scattering on many disks in the model (D2) with noise and dissipation. We see that for $j = 2.25$ orbits are captured in the vicinity of the center of nonlinear resonance at $\phi' \approx 0$ well seen in Fig. 8. For $j = 2.1$ we have a density maximum located at smaller values of $v_{\rm res}$ and $\phi' \approx 0$ even if there is a

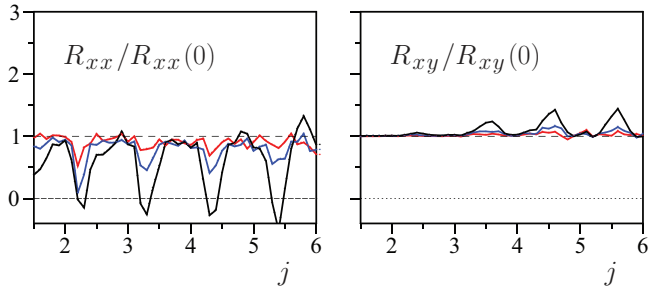

FIG. 14. (Color online) Same as in Fig. 13 at various microwave amplitudes $\epsilon = 0.01$ (red/gray curve), 0.02 (blue/dark curve), 0.04 (black curve); amplitude of noise is fixed at $\alpha_i = 0.005$. Data for model (D2).

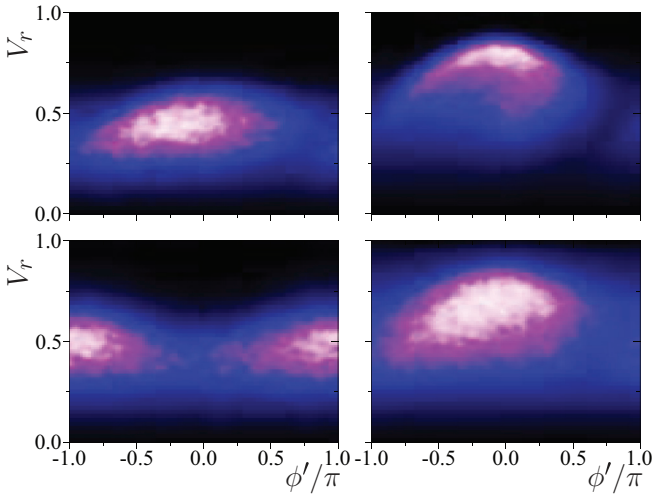

FIG. 15. (Color online) Phase space (v_r,ϕ') of trajectories at the moment of collisions with disks for parameters of Fig. 14 at $\epsilon = 0.04$: $j = 2.1$ (top left), $j = 2.25$ (top right), $j = 2.75$ (bottom left), $j = 3.25$ (bottom right). Here $\phi' = \phi - \theta$ where $\phi = \omega t$ is a microwave phase at the moments of collisions with disk and θ is the angle on disk at collision moment, counted from x axis (same as in Figs. 7, 8). Data are obtained from 500 trajectories iterated up to time $t = 10^6/\omega$. Density of points is shown by color with black at zero and white at maximum density. The average number of collisions per disk per trajectory is $N_{\rm col} = 12.4$, 25.9, 9.5, 15.5 respectively for $j = 2.1$, 2.25, 2.75, 3.75. Data are obtained for model (D2).

certain shift of $v_{\rm res}$ produced by a significant resonance width at $\epsilon = 0.04$. At $j = 2.75$ we have a density maximum at $\phi' \approx \pm\pi$ corresponding to an unstable fixed point of separatrix. The total number of collision points $N_{\rm col}$ in this case is by a factor 2.5 smaller than in the case of stable fixed point at $j = 2.25$. A similar situation is seen in the case of wall model (W1) [see Figs. 1(d) and 1(f) in Ref. 9] even if there the ratio between the number of captured points was significantly larger. The results of Fig. 15 show that in the ZRS phase the collisions with disk indeed create synchronization of cyclotron and microwave phases and capture of trajectories inside the nonlinear resonance.

However, there are also some distinctions between bulk disk model (D2) and experimental observations. The first one is that there are minima for $R_{xx}/R_{xx}(0)$ but there are no peaks which are very visible around integer j values in ZRS experiments,[1,2,8] and numerical simulations of transport along the edge.[9] The second one is the appearance of small negative values of R_{xx} at j_r values.

We attribute the absence of peaks to a specific dissipation mechanism which takes place only at disk collisions. It is rather convenient to run long trajectories using the exact solution for free propagation between disks. Indeed, in this scheme there is no dissipation during this free space propagation and thus these parts of trajectories have no displacement along the static field. We also tested a dissipation model with additional $\gamma(v) = \gamma_0(|v/v_F|^2 - 1)$ for $|v| > v_F$ and $\gamma(v) = 0$ for $|v| \leqslant v_F$. This dissipation works only in the disk vicinity when the distance between disk center and cyclotron center is smaller than $r_d + r_c$. The dissipation γ_d on the disk remains unchanged. We also added a certain roughness of disk surface modeled

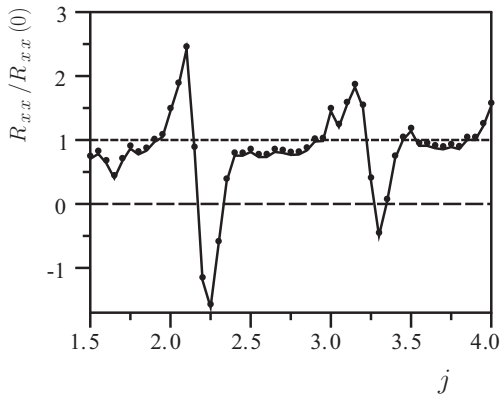

FIG. 16. Dependence of $R_{xx}/R_{xx}(0)$ on j in the disk model with dissipation at disk collisions at rate $\gamma_d = 0.01$ and dissipation in disk vicinity with rate $\gamma_0/\omega = 0.02$; a disk roughness gives additional angle rotations with amplitude $\alpha_d = 0.1$ (see text); the amplitude of noise in disk vicinity is $\alpha_i = 0.001$. Here we have $\epsilon = 0.04$, $\epsilon_s = 0.001$; 51 numerical points in j are connected by lines to guide the eye. Data are obtained by averaging over 100 trajectories propagating up to time $t = 10^6/\omega$. Data for model (D3).

as an additional random angle rotation of velocity vector in the range $\pm\alpha_d$, done at the moment of collision with the disk. We call this system disk model (D3). The results for the resistivity ratio $R_{xx}/R_{xx}(0)$ are shown in Fig. 16. They show an appearance of clear peaks of $R_{xx}/R_{xx}(0)$ in the presence of such additional dissipation in the vicinity of integer j. There is also a small shift of minima from integer plus $1/4$ to integer plus 0.4–0.5.

The second point of distinction from ZRS experiments is a small negative value of R_{xx} at resonant j values. It is relatively small for disk model (D2) (see Figs. 13, 14) and it becomes more pronounced for disk model (D3) (see Fig. 16). It is possible that a scattering on the disk in the presence of dissipation, noise, static, and microwave field gives a negative displacement Δx which generates such negative R_{xx} values. We expect that in the limit of static field going to zero this effect disappears. Indeed, the negative values become smaller at smaller ϵ_s according to the data of Fig. 11 but unfortunately the small ϵ_s limit is also very difficult to investigate numerically.

We consider that at this stage of the theory the presence of negatives values for R_{xx} does not constitute a critical disagreement. The escape parameters for electrons that have been captured on an impurity for a time long enough to make many rotations around it are likely to strongly depend on the model for the electron impurity interaction and further theoretical work on a more microscopic model is needed. In general a zero average displacement along the field direction seems natural for a smooth distribution of trapping times with a characteristic time scale much larger than the rotation time around the impurity (this assumption does not seem to hold for our model; see for example the sharp features on Fig. 10). Finally in Sec. VII we propose a slightly different mechanism by which the combination of trapping on impurities investigated here and electron-electron interactions can lead to ZRS.

V. PHYSICAL SCALES OF ZRS EFFECT

The ZRS experiments[1,2] show that the resistance R_{xx} in the ZRS minima scales according to the Arrhenius law $R_{xx} \propto \exp(-T_0/T)$ with a certain energy scale dependent on the strength of microwave field. In typical experimental conditions one finds very large $T_0 \approx 20$ K at $j_r = 5/4$ (see, e.g., Fig. 3 in Ref. 2). These data also indicate the dependence $T_0 \propto 1/j_r \propto B$. This energy scale $k_B T_0$ is very large being only by a factor 7 smaller than the Fermi energy $E_F/k_B \approx 150$ K. At the same time the amplitude of the microwave field is rather weak corresponding to $\epsilon \approx 0.003$ at a field of 1 V/cm or ten times larger at 10 V/cm (unfortunately it is not known what is the amplitude of the microwave field acting on an electron).

As in Ref. 9 we argue that the Arrhenius scale is determined by the energy resonance width (4) with $T_0 = E_r/k_B$. Indeed, the resonance forms an energy barrier for a particle trapped inside the resonance by dissipative effects being analogous to a washboard potential. An escape from this potential well requires overcoming the energy E_r leading to the Arrhenius law for R_{xx} dependence on temperature. Assuming the case of the wall with $\rho = 1$ we obtain at $E = 3$ V/cm the activation temperature $T_0 \approx 23$ K, in satisfactory agreement with the experimental observations. The theoretical relation (4) also reproduces the experimental dependence $T_0 \propto 1/j_r$ at $\rho = 1$. In this relation $T_0 \propto \epsilon \propto E$ is confirmed by the numerical simulations presented in Ref. 9. This dependence is in satisfactory agreement with the power dependence found in experiments.[1] In other samples one finds that the dependence $T_0 \propto \epsilon^2$ works in a better way. We think that higher terms in a nonlinear resonance can be responsible for scaling $T_0 \propto \epsilon^2$ being different from the relation (4). Also a finite rigidity of the wall or disk scatterers can be responsible for the appearance of the higher power of ϵ.

The energy scale E_r on disks is enhanced by a factor $\rho = 1 + r_c/r_d$ for the case of radial field (4). However, we showed that for a linear polarization the scale E_r is given by Eq. (5) and thus there is no enhancement at large ρ. Indeed, we performed direct simulations at parameters of Fig. 14 with the reduced value of disk radius by a factor 2. The numerical data give approximately the same traces $R_{xx}/R_{xx}(0)$ vs j at $\epsilon = 0.01, 0.02, 0.04$ without visible signs of deeper minima at small ϵ. This confirms the theoretical expressions (5). In any case, for small values $r_d \ll r_c$ one should analyze the quantum scattering problem which is significantly more complex compared to the classical case. We may assume that in a quantum case one should replace r_d by a magnetic length $a_B \approx r_c/\sqrt{v} \propto \sqrt{B}$. In such a case we are getting $\rho = 1 + \sqrt{v} \approx 9$ that gives $T_0 \approx 8$ K at $j \approx 2.25$ and microwave amplitude $E \approx 3$ V/cm. However, in this case we obtain the scale T_0 being practically independent of j which differs from experimental data. In any case in experiments the size of impurities is small compared to r_c and a quantum treatment is required to reproduce the correct picture for R_{xx} dependence on parameters in the ZRS phase.

Another point is related to the positions of ZRS minima on j axis. We recall that for the wall model the resonance is located at $v_{\rm res} = \pi\delta j/j$ (4) and that the separatrix width is $\delta v = 4\sqrt{\epsilon/j}$. The capture of trajectories from the bulk is most efficient when a half width of separatrix touches the border

of bulk at $v_r = 0$ with $v_{\rm res} = \delta v/2$ that gives the expression $\delta j_\epsilon = 2\sqrt{\epsilon j}/\pi$ for the wall case. At $\epsilon = 0.06$, $j = 2.25$ this gives $\delta j_\epsilon = 0.22$ being in a good agreement with the numerical data $\delta j \approx 1/4$ for R_{xx} dependence on j (see Figs. 2, 3 in Ref. 9 with a visible tendency of δj growth with j). For the data presented here in Fig. 14 for the disk case at $\epsilon = 0.04$, $\rho = 1 + j$, $j = 2.25$ we obtain from (5) $\delta j_\epsilon = 0.11$ that is slightly less than the numerical value $\delta j \approx 0.25$ for minima location. We attribute this difference to an approximate nature of expression for the resonance width at relatively strong microwave fields. We also note that in experiments an additional contribution to the value of δj can appear due to a finite rigidity of disk and wall potentials.

VI. THEORETICAL PREDICTIONS FOR ZRS EXPERIMENTS

The theoretical models presented here and in Ref. 9 reproduce the main experimental features of ZRS experiments.[1,2,8] However, it would be useful to have some additional theoretical predictions which can be tested experimentally. A certain characteristic feature of both wall and disk models is the appearance of nonlinear resonance. For example, according to the wall model (W2) described by Eq. (3) the dynamics inside the resonance is very similar to dynamics of a pendulum. The frequency of phase oscillations inside the resonance is $\Omega_{ph} = \sqrt{K} = 2\sqrt{\epsilon\omega/\omega_c} = 2\sqrt{\epsilon j} \ll 1$.[13] Here the frequency is expressed in the number of map iterations and since the time between collisions is approximately $2\pi/\omega_c$ we obtain the physical frequency Ω_r of these resonant oscillations being $\Omega_r/\omega = \Omega_{ph}\omega_c/(2\pi\omega) = \sqrt{\epsilon\omega_c/\omega}/\pi$. At $\epsilon \sim 0.02$ this frequency is significantly smaller than the driving microwave frequency. The dynamics inside the resonance should be very sensitive to perturbations at frequency $\omega_1 \approx \Omega_r$ that gives

$$\omega_1/\omega = \sqrt{\epsilon\omega_c/\omega}\,/\pi. \tag{6}$$

To check this theoretical expectation we study numerically the effect of additional microwave driving with dimensional amplitude ϵ_1 ($\epsilon_1 \ll \epsilon$) and frequency ω_1. We use the wall model (W2) based on the Chirikov standard map described here and in Ref. 9. As for the additional driving frequency we have $\epsilon_1 = |E_1|/(\omega_1 v_F)$ where E_1 is the field strength of microwave frequency ω_1; we assume that both main and additional fields are collinear and perpendicular to the wall. In the presence of the second frequency the map (3) takes the form

$$\begin{aligned} \bar{v}_y &= v_y + 2\epsilon\sin\phi + 2\epsilon_1\sin(\omega_1\phi/\omega) + I_{cc}, \\ \bar{\phi} &= \phi + 2(\pi - \bar{v}_y)\omega_/\omega_c. \end{aligned} \tag{7}$$

The only modification appears in the first equation since now the change of velocity at collision depends on both fields; the second equation remains the same as in (3). As in model (W2) the term I_{cc} describes the effects of dissipation with rate γ_c and noise with amplitude α of random velocity angle rotations. We call this system model (W3).

In model (W3) the resistance R_{xx} is computed numerically in the same way as in model (W2) described in Ref. 9: The displacement along the edge between collisions is $\delta x = 2v_y/\omega_c$; it determines the total displacement Δx along the edge during the total computation time $\Delta t \sim 10^4/\omega$; then $R_{xx} \propto 1/D_x = \Delta t/(\Delta x)^2$ where D_x is an effective diffusion rate along the edge. To see the effect of additional weak test driving ϵ_1 at frequency ω_1 we place the system in the ZRS phase at $j = \omega/\omega_c = 2.25$ and measure the variation of rescaled resistance $R_{xx}/R^\epsilon_{xx}(0)$. Here R_{xx} is the resistance in the presence of both microwave fields ϵ and ϵ_1 while $R^\epsilon_{xx}(0)$ is the resistance at $\epsilon_1 = 0$ and a certain fixed ϵ. The dependence of $R_{xx}/R^\epsilon_{xx}(0)$ on the frequency ratio is shown in Fig. 17 in the left panel. The main feature of this data is the appearance of a peak at low frequency ratio $\omega_1/\omega < 0.1$. In the range $0.1 < \omega_1/\omega < 0.4$ the testing field ϵ_1 is nonresonant and does not affect R_{xx}; however at $\omega_1/\omega < 0.1$ it becomes resonant to the pendulum oscillations in the wall vicinity and hence strongly modifies the R_{xx} value. The dependence of this resonance ratio ω_1/ω on the amplitude of the main driving field ϵ is shown in the right panel of Fig. 17. The numerical data are in a good agreement with the above theoretical expression (6).

The theoretical dependence (6) allows us to check the synchronization theory of edge state stabilization. It also allows us to measure the strength of the main microwave driving force acting on an electron that still remains an experimental challenge. The experimental testing of relation (6) requires working with good ZRS samples which have very low resistance in ZRS minima since this makes the effect of testing field ω_1 more visible. We note that the recent experiments in a low-frequency regime $\omega/\omega_c \ll 1$[24] demonstrate that R_{xx} is sensitive to low-frequency driving. The expression (6) is written for the case when R_{xx} is mainly determined by transport along edges. If the dominant contribution is given by bulk disk scatterers then a certain numerical coefficient A should be introduced in the right part of the expression. According to the data of Fig. 8 and Eqs. (5) we estimate $A \approx 0.5$ (the separatrix width is smaller for the disk case compared to the wall case at the same ϵ).

Another interesting experimental possibility of our theory verification is to take a Hall bar of a high-mobility 2DEG sample and put on it antidots with regular or disordered distribution (it is important to have no direct collisionless path for a cyclotron radius in crossed dc electric and magnetic fields) with a low density of antidot disks $n_d r_d^2 \ll 1$ (as in our numerical studies) so that an average distance between antidots is larger than the cyclotron radius r_c. The regular antidot lattices have been already realized experimentally.[18,19] The effect of microwave field on electron transport in a regular lattice has been studied in the frame of ratchet transport in asymmetric lattices.[25] Even a case of symmetric circular antidots has been studied in Ref. 25 but the lattice was regular and no special attention was paid to analysis of resistivity at the ZRS resonant regime with $j \approx j_r$. The earlier studies of the combined effect of microwave and magnetic fields on 2DEG transport on a circular antidot lattice have been also reported in Ref. 26. However, in Ref. 26 the experiments were done in the regime when the number of antidots N_a inside the cyclotron circle area is larger than unity, while the conditions of ZRS experiments correspond to $N_a \ll 1$. We think that the experimental conditions of Refs. 25,26 can be relatively easy modified to observe the ZRS effect on disk scatterers discussed here.

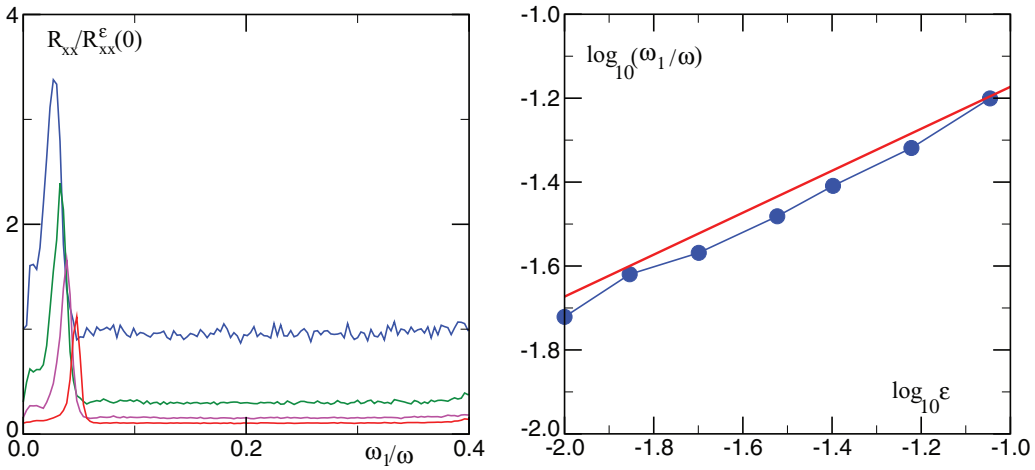

FIG. 17. (Color online) Left panel: Dependence of rescaled resistance $R_{xx}/R^{\epsilon}_{xx}(0)$ on frequency ratio ω_1/ω in model (W3) described by the map (7). Here, the test driving at frequency ω_1 has fixed amplitude $\epsilon_1 = 0.007$; the main microwave driving is located in the ZRS phase at $j = \omega/\omega_c = 2.25$, and its amplitude takes values $\epsilon = 0.02$ (blue curve), 0.03 (green curve), 0.04 (magenta curve), 0.06 (red curve) (these curves follow from top to bottom at $\omega_1/\omega = 0.2$). The values of R_{xx} are computed at fixed $\epsilon_1 = 0.007$ and corresponding ϵ; the values of $R^{\epsilon}_{xx}(0)$ are computed at $\epsilon_1 = 0$ and $\epsilon = 0.02$. The data are obtained at noise amplitude $\alpha = 0.02$ and dissipation $\gamma_c = 0.01$; averaging is done over 2000 trajectories for 5000 iterations of map (7). Right panel: Dependence of peak position ω_1/ω on main microwave driving amplitude ϵ obtained from data of left panel at $\epsilon_1 = 0.007$ and additional data at $\epsilon_1 = 0.003$ (blue points), the theory dependence (6) at $\omega/\omega_c = 2.25$ is shown by the straight red line. Data for model (W3).

VII. DISCUSSION

Above we presented theoretical and numerical results which in our opinion explain the appearance of microwave-induced ZRS in high-mobility samples. The synchronization theory of ZRS proposed in Ref. 9 and extended here is based on a clear physical picture: High harmonics $\omega/\omega_c = j > 1$ are generated by collisions with a sharp edge boundary or isolated impurities which are modeled here by specular disks. The ZRS phases appear in the vicinity of resonant values $j_r \approx 1 + 1/4, 2 + 1/4, \ldots$. At these j_r values the cyclotron phase of electron motion becomes synchronized with the microwave phase due to dissipative processes present in the system.

For trajectories at the edge vicinity this synchronization gives stabilization of propagation along edge channels that creates an exponential drop of resistivity contribution of these channels with decreasing amplitude of thermal noise and increasing amplitude of microwave field. The contribution to resistivity from trajectories in the bulk is analyzed in the frame of scattering on many well-separated disk impurities. Here again the synchronization of cyclotron phase with the microwave phase takes place approximately at the same resonant j_r values. At these j_r values the synchronization leads to long-time capture of trajectories in the disk vicinity. During this long time an initial cyclotron phase is washed out by noisy fluctuations and many rotations around the disk and thus an electron escapes from a disk with an average zero displacement along the applied dc field even if dynamics in the disk vicinity is dissipative. This provides the main mechanism of suppression of dissipative resistivity contribution from isolated impurities in the bulk. As a result the contribution of bulk to dissipative conductivity σ_{xx} is suppressed, as was assumed in Ref. 9, and the main contribution to current is given by electron propagation along edge states stabilized by a microwave field.

As we showed above the resonance width or resonance energy scale E_r are approximately the same for the disk and wall cases [see Eqs. (4), (5)]. We note that for the disk case the energy E_r is not sensitive to the disk radius as soon as it is significantly smaller than the cyclotron radius. Thus we expect that at j_r values the conductivity σ_{xx} in the bulk is suppressed by a microwave field and at these fields the current is flowing essentially along stabilized edge states. In the case of Corbino geometry we have radial conductivity σ_{rr} which is determined by the bulk scattering and now the minima of σ_{rr} are located at j_r values (see, e.g., Figs. 12, 13, and 14 where $R_{xx} \propto \sigma_{xx} \sim \sigma_{rr}$). The ZRS experiments performed in the Corbino geometry give minima of σ_{rr} at these j_r values (see, e.g., Refs. 27 and 28) being in agreement with the synchronization theory.

It is interesting to note that the nonlinear dynamics in the vicinity of the edge and disk impurity is well described by the Chirikov standard map.[13] The map description explains the location of resonances at integer values of j with an additional shift $\delta j \approx 1/4$ produced by a finite separatrix width of nonlinear resonance. A finite rigidity of wall or disk potential can give a modification of this shift δj.

Our results show that the ZRS phases at j_r appear only at weak noise corresponding to high-mobility samples. Strong noise destroys synchronization and trajectories are no longer captured at edge or disk vicinity. We also note that internal sample potentials with significant gradients act like a strong local dc field which destroys stability regions around disk impurities or near the edge. Thus the ZRS effect exists only in high-mobility samples. The resistance at ZRS minima drops significantly with the growth of microwave field strength since it increases the amplitude of nonlinear resonance which captures the synchronized trajectories.

The synchronization theory of ZRS is based on classical dynamics of noninteracting electrons. It is possible that

electron-electron interaction effects can also suppress the contribution to resistivity from neutral short-range scatterers (interface roughness, adatoms, etc.). Indeed, long capture times can increase the electron density around these short-ranged impurities transforming them into long-range charged scatterers that the other electrons can circumvent by adiabatically following the long-range component of the disorder potential thereby avoiding a scattering event. However, the theoretical description of this short-ranged impurity cloaking mechanism for the ZRS effect remains a serious challenge.

Another important step remains the development of a quantum synchronization theory for ZRS. Even if in experiments the Landau level is relatively high $\nu \sim 60$, there are only about ten Landau levels inside a nonlinear resonance[9] and quantum effects should play a significant role. The general theoretical studies show that the phenomenon of quantum synchronization persists at small effective values of Planck constant $\hbar_{\rm eff}$ but it becomes destroyed by quantum fluctuations at certain large values of $\hbar_{\rm eff}$.[29]

The importance of quantum ZRS theory is also related to the short-range nature of the impurities considered here, typically on a scale of a few nanometers or even less. We have modeled these impurities by disks with a radius that was only several times (in fact j times) smaller than the cyclotron radius which is not so close to microscopic reality. We could argue that in the quantum case a nanometer-sized impurity would act effectively as an impurity of a size of quantum magnetic length $a_B \sim r_c/\sqrt{\nu} \approx r_c/8 \sim 100$ nm. This gives a ratio $r_c/a_B \sim 8$ which is comparable with the one used in our simulations with $r_c/r_d = j \sim 7$ but of course a quantum treatment of scattering on nanometer-size impurities in crossed electric and magnetic and also microwave fields remains a theoretical challenge. We note that such type of scattering can be efficiently analyzed by tools of quantum chaotic scattering (see, e.g., Refs. 30,31) and we expect that these tools will allow us to make progress in the quantum theory development of striking ZRS phenomenon. We hope that the synchronization theory of microwave-induced ZRS phenomenon described here can be tested in further ZRS experiments.

ACKNOWLEDGMENTS

This work was supported in part by ANR France PNANO project NANOTERRA; O.V.Z. was partially supported by the Ministry of Education and Science of the Russian Federation.

[1] R. G. Mani, J. H. Smet, K. von Klitzing, V. Narayanamurti, W. B. Johnson, and V. Umansky, Nature (London) **420**, 646 (2002).
[2] M. A. Zudov, R. R. Du, L. N. Pfeiffer, and K. W. West, Phys. Rev. Lett. **90**, 046807 (2003).
[3] S. I. Dorozhkin, JETP Lett. **77**, 577 (2003).
[4] J. H. Smet, B. Gorshunov, C. Jiang, L. Pfeiffer, K. West, V. Umansky, M. Dressel, R. Meisels, F. Kuchar, and K. von Klitzing, Phys. Rev. Lett. **95**, 116804 (2005).
[5] A. A. Bykov, A. K. Bakarov, D. R. Islamov, and A. I. Toropov, JETP Lett. **84**, 391 (2006).
[6] D. Konstantinov and K. Kono, Phys. Rev. Lett. **105**, 226801 (2010).
[7] D. Konstantinov, A. D. Chepelianskii, and K. Kono, J. Phys. Soc. Jpn. **81**, 093601 (2012).
[8] I. A. Dmitriev, A. D. Mirlin, D. G. Polyakov, and M. A. Zudov, Rev. Mod. Phys. **84**, 1709 (2012).
[9] A. D. Chepelianskii and D. L. Shepelyansky, Phys. Rev. B **80**, 241308(R) (2009).
[10] A. Pikovsky, M. Rosenblum, and J. Kurths, *Synchronization: A Universal Concept in Nonlinear Sciences* (Cambridge University Press, Cambridge, 2001).
[11] A. D. Chepelianskii, arXiv:1110.2033.
[12] W. G. Hoover, *Time Reversibility, Computer Simulation, and Chaos* (World Scientific, Singapore, 1999).
[13] B. V. Chirikov, Phys. Rep. **52**, 263 (1979).
[14] A. J. Lichtenberg and M. A. Lieberman, *Regular and Chaotic Dynamics* (Springer, Berlin, 1992).
[15] B. Chirikov and D. Shepelyansky, Scholarpedia **3**(3), 3550 (2008).
[16] Y. Avishai and G. Montambaux, Eur. Phys. J. B **79**, 215 (2011).
[17] F. Benvenuto, G. Casati, I. Guarneri, and D. L. Shepelyansky, Z. Phys. B **84**, 159 (1991).
[18] D. Weiss, M. L. Roukes, A. Menschig, P. Grambow, K. von Klitzing, and G. Weimann, Phys. Rev. Lett. **66**, 2790 (1991).
[19] G. M. Gusev, V. T. Dolgopolov, Z. D. Kvon, A. A. Shashkin, V. M. Kudryashov, L. V. Litvin, and Yu. Nastaushev, Pis'ma Zh. Eksp. Teor. Fiz. **54**, 369 (1991).
[20] R. Fleischmann, T. Geisel, and R. Ketzmerick, Phys. Rev. Lett. **68**, 1367 (1992).
[21] T. Geisel, R. Ketzmerick, and O. Schedletzky, Phys. Rev. Lett. **69**, 1680 (1992).
[22] N. Berglund, A. Hansen, E. H. Hauge, and J. Piasecki, Phys. Rev. Lett. **77**, 2149 (1996).
[23] A. D. Chepelianskii and D. L. Shepelyansky, Phys. Rev. B **63**, 165310 (2001).
[24] A. D. Chepelianskii, J. Laidet, I. Farrer, H. E. Beere, D. A. Ritchie, and H. Bouchiat, Phys. Rev. B **86**, 205108 (2012).
[25] S. Sassine, Yu. Krupko, J.-C. Portal, Z. D. Kvon, R. Murali, K. P. Martin, G. Hill, and A. D. Wieck, Phys. Rev. B **78**, 045431 (2008).
[26] E. Vasiliadou, R. Fleischmann, D. Weiss, D. Heitmann, K. v. Klitzing, T. Geisel, R. Bergmann, and H. Schweizer, Phys. Rev. B **52**, R8658 (1995).
[27] C. L. Yang, M. A. Zudov, T. A. Knuuttila, R. R. Du, L. N. Pfeiffer, and K. W. West, Phys. Rev. Lett. **91**, 096803 (2003).
[28] A. A. Bykov, JETP Lett. **87**, 551 (2008).
[29] O. V. Zhirov and D. L. Shepelyansky, Eur. Phys. J. D **38**, 375 (2006).
[30] J. Wiersig and M. Hentschel, Phys. Rev. Lett. **100**, 033901 (2008).
[31] A. Eberspächer, J. Main, and G. Wunner, Phys. Rev. E **82**, 046201 (2010).